Coastal Engineering, 19 (1993) 263–282
Elsevier Science Publishers B.V., Amsterdam

A comparison of two spectral wave models in the Southern California Bight

W.C. O'Reilly* and R.T. Guza
Center for Coastal Studies, Scripps Institution of Oceanography, La Jolla, CA 92093, USA

(Received 6 April 1992; accepted after revision 3 September 1992)

ABSTRACT

Two models, a spectral refraction model (Longuet-Higgins) and a parabolic equation method (PEM) refraction-diffraction model (Kirby), are used to simulate the propagation of surface gravity waves across the Southern California Bight. The Bight contains numerous offshore islands and shoals and is significantly larger ($\approx$300 km by 300 km) than regions typically studied with these models. The effects of complex bathymetry on the transformation of incident wave directional spectra, $S_0(f,\theta_0)$, which are very narrow in both frequency and direction are difficult to model accurately. As $S_0(f,\theta_0)$ becomes broader in both dimensions, agreement between the models improves and the spectra predicted at coastal sites become less sensitive to errors in the bathymetry grid, to tidal changes in the mean water depth, and to uncertainty in $S_0(f,\theta_0)$ itself. The smoothing associated with even relatively narrow (0.01 Hz–5° bandwidth) $S_0(f,\theta_0)$ is usually sufficient to bring the model predictions of shallow water energy into at least qualitative agreement. However, neither model is accurate at highly sheltered sites. The importance of diffraction degrades the predictions of the refraction model, and a positive bias [O(10%) of the deep ocean energy] in the refraction-diffraction model estimates, believed to stem from numerical "noise" (Kirby), may be comparable to the low wave energy. The best agreement between the predicted spectra generally occurs at moderately exposed locations in deeper waters within the Bight, away from shallow water diffractive effects and in the far-field of the islands. In these cases, the differences between the models are small, comparable to the errors caused by tidal fluctuations in water depth as waves propagate across the Bight. The accuracy of predicted energies at these sites is likely to be limited by the uncertainty in specifying $S_0(f,\theta_0)$.

1. INTRODUCTION

The Southern California Bight extends from approximately 32°N to Point Conception (34.5°N) on the west coast of the U.S. (Fig. 1). Numerous offshore islands, shallow banks, and coastal submarine canyons partially shelter the coastline from deep ocean surface gravity waves. As a result, the wave climate within the Bight is spatially complex due to the reflection, refraction, diffraction, and dissipation of the incident deep ocean wave energy (Munk and Traylor, 1947; Arthur, 1951; Emery, 1958; Pawka, 1982, 1983). Engineering studies commonly use refraction models to examine wave propaga-

*Corresponding author.

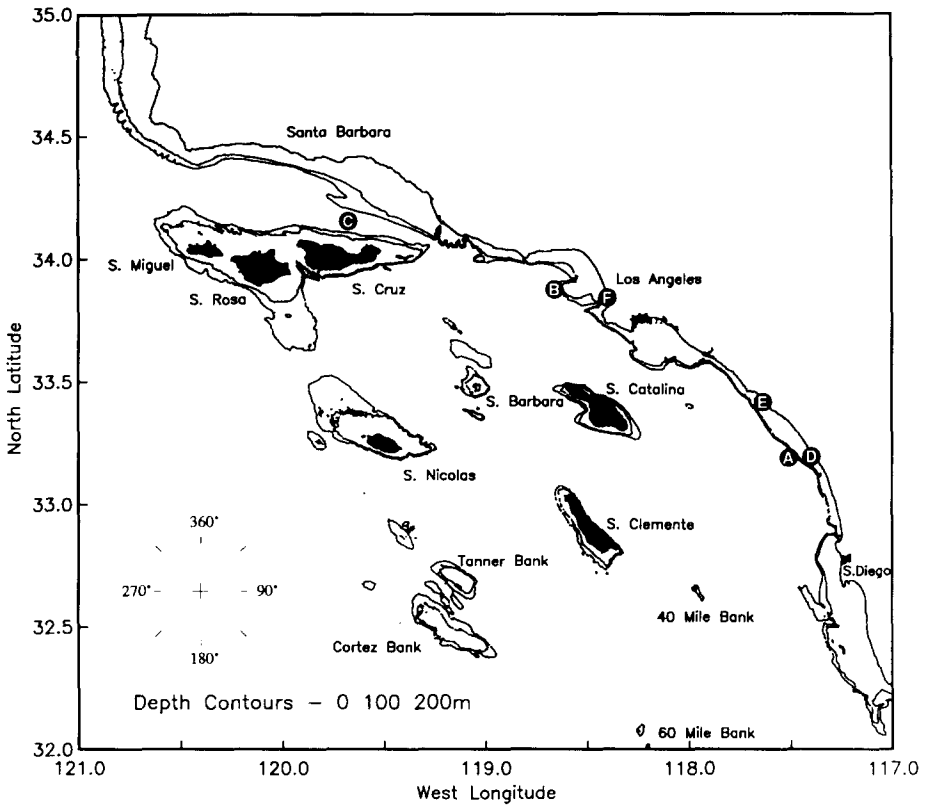

Fig. 1. Shallow water bathymetry of the Southern California Bight. Wave propagation models are compared at sites A–F, in local deep water (depth = 300 m; A = Oceanside, B = Santa Monica, C = Santa Barbara) and shallow water (depth = 10 m; D = Oceanside Beach, E = San Clemente Beach, F = Redondo Submarine Canyon).

tion in areas as large as the Bight ($\approx$300 km by 300 km), even when diffraction is not necessarily negligible. However, wave propagation models including both refraction and diffraction are computationally intensive, requiring a supercomputer for large areas, and can be numerically noisy. Conditions for which refraction and refraction–diffraction model solutions agree are therefore of practical interest.

Two existing linear wave propagation models, spectral refraction (R model, Longuet-Higgins, 1957; LeMehaute and Wang, 1982) and spectral refraction–diffraction (RD model, Kirby, 1986a; Izumiya and Horikawa, 1987; Isobe, 1987), were compared in O'Reilly and Guza (1991) for simple bathymetries. Our present focus is on the application of these models to the entire Southern California Bight. We assume that the deep ocean wave spectrum is spatially homogeneous outside the islands, and that there is no wave generation by local winds. Therefore, the present results concern relatively low fre-

quency swell ($f \approx 0.04$–0.10 Hz) from distant storms. Tidal and other large scale currents in the Bight are typically less then 30 cm/s, too weak to have a large effect on long period waves, and are not included. In addition, nonlinear effects are assumed negligible because propagation distances within the Bight are too short for significant spectral evolution in deep water, the shelf is narrow, and model solutions in very shallow water (< 10 m) are not sought. Our overall objective is to discuss the application of R and RD models in engineering studies of the sheltering effects of islands and shoals over spatial scales of several 100 km.

2. THE SOUTHERN CALIFORNIA BATHYMETRY GRID

A detailed bathymetry grid is required to model wave propagation in the Bight. Depth soundings from the National Ocean Survice (NOS) digital database, for latitudes between 32°–35°N and longitudes between 117°–122°W, were used to create a 3 by 3 second bathymetry grid (77.2 m by 92.6 m at 33.5°N) for the depth range 0–300 m. The Delaunay tesselation method of Watson (1982) produced a network of triangles with the sounding locations at their vertices. (Delaunay triangles have the property that no vertex lies inside the circumcircle of any triangle. Hence, the network is as close to equiangular as possible.) The water depth at each grid point was then calculated by linear interpolation from the plane passing through the vertices of the triangle containing that point. Surveys in the NOS database extended from the 1930's to the 1980's. In areas where surveys overlapped, the most recent survey was used. There was little coastal data available for the region south of the U.S.–Mexico border (≈ 32.5°N) to 32°N latitude, so relatively low resolution, hand digitized contours from bathymetric maps were used. The completed grid was screened for bad points through a comparison to NOS nautical charts.

A small amount of grid distortion results when a simple transformation, equivalent to a Mercator projection of the latitude–longitude grid centered on 35.5°N latitude, is used in the conversion to Cartesian coordinates. While the distance between lines of longitude on a sphere decrease with increasing latitude, this distance remains constant under the present transformation, and results in a maximum grid spacing error of 2.5% at the north and south ends of the grid. Wave propagation errors arise from the fact that waves do not travel along great circle paths on the grid, except when propagating directly along the y-axis (North-South), but the maximum directional errors due to grid distortion are acceptably small (≈ 1°).

3. THE SPECTRAL REFRACTION–DIFFRACTION MODEL

The refraction–diffraction model used here is the linear version of the higher order PEM (Padé approximant) model (Kirby 1986a,b; Kirby and Dalrym-

ple, 1986). The model is for a monochromatic and unidirectional wave train, but monochromatic results can be combined to simulate wave spectra (Izumiya and Horikawa, 1987; Isobe, 1987; Panchang et al., 1990). RD model calculations in the Bight are numerically intensive. For example, for a frequency of 0.06 Hz, the grid has dimensions of approximately 15,000 by 13,000 points and the number of numerical calculations are 10^4 larger than typical problems solved using parabolic RD models (e.g. Kirby and Dalrymple, 1986). RD model runs are therefore performed on a Cray Y-MP supercomputer and large gains in computational efficiency are made by simultaneously evaluating a range of incident wave directions, at a single frequency, through the "vectorization" of the program code. The solution for 45 incident wave directions and a wave frequency of 0.06 Hz requires 45 to 65 cpu minutes depending on the grid orientation. Higher wave frequencies have shorter wavelengths and result in smaller grid spacings and more cpu time. For example, the same model runs at a wave frequency of 0.10 Hz use from 135 to 190 cpu minutes. As discussed below, several thousand frequency-directional combinations are needed to span the range of realistic wave conditions, so the total cpu time is significant. Since the RD model is linear, the solution need only be calculated once for each frequency and direction, with an incident wave of unit amplitude. The response to a specific incident directional spectrum is then constructed by appropriately weighting each discrete component.

3.1. Minimizing high-angle RD wave propagation errors

The Southern California Bight is exposed to a wide range of possible incident wave directions. However, PEM refraction-diffraction models are unable to accurately propagate wave energy at high angles to the x-axis of the bathymetry grid [> 55–$60°$ for the Kirby (1986a) model incorporated here]. To minimize high-angle errors in the Southern California RD model solutions, four separate grid orientations are used. Two separate bathymetry grids are derived from the previously described 3 second by 3 second NOS bathymetry grid, using bilinear interpolation; one is for waves from the south or west, and the other for waves from the southwest or northwest (the x and y axes can be switched in each case to produce four different orientations). The west and south grid orientations have a grid spacing of 100 m and the southwest and northwest grid have a spacing of 70.71 m. The grid step sizes used in the refraction-diffraction calculations are an integer fraction of this grid spacing and $\leq 1/6$th of a wavelength in 10 m of water. The grid dimensions are chosen such that all the orientations have common grid points at a 100 m spacing. Model solutions at these points thus include the full range of deep ocean wave directions, each performed over the grid that minimizes high-angle wave propagation (initial deep ocean angles $\pm 22.5°$ from the x-axis are evaluated for each of the orientations).

3.2. The dissipation of wave energy along coastlines

The majority of the remotely generated wave energy propagating into the Bight is dissipated by wave breaking near the Southern California coastline and the offshore islands. The details of this dissipative process are not important to the present study of wave energy in depths > 10 m, outside the surfzone. Therefore, areas with water depths less than 5 meters are considered "dissipative regions" and energy entering these depths is numerically absorbed. This method (Dalrymple et al., 1984) introduces relatively little numerical noise into the RD model when compared to specific wave breaking algorithms (for example, Kirby and Dalrymple, 1986). The dissipation rate is controlled by a dissipation coefficient and a value of 0.05 is used here. Most of the dissipative regions are many wavelengths wide and a large range of dissipation coefficients effectively remove the wave energy propagating into these areas.

3.3. Estimating energy transfer functions

The linear wave models are used to estimate energy transfer functions,

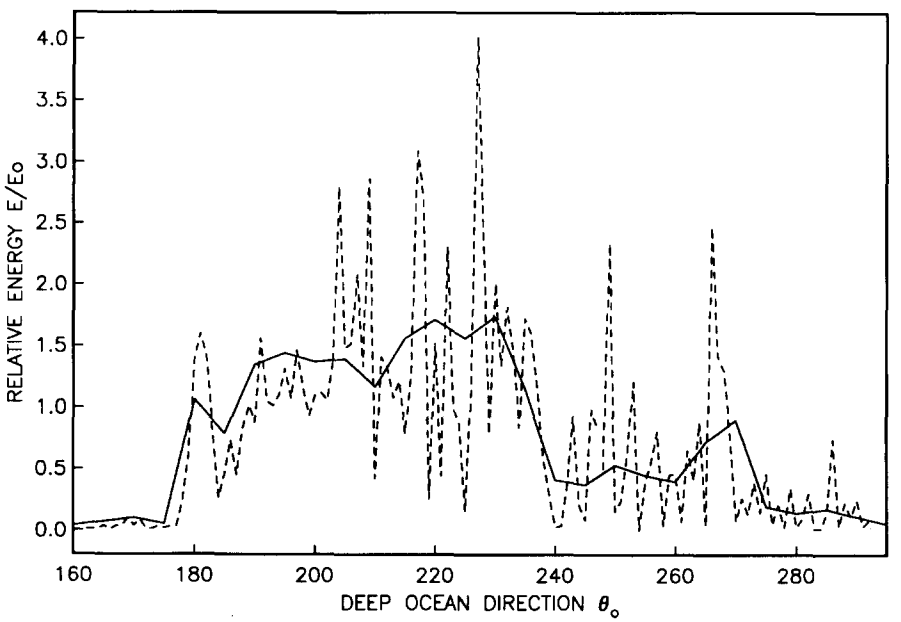

Fig. 2. Comparisons of RD model energy transfer functions (Eq. 1) at Oceanside Beach (Site D, Fig. 1) for a monochromatic (f=0.06 Hz), unidirectional wave (dashed line) and a narrow rectangular (0.01 Hz–5°) frequency-directional spectrum (solid line). The deep ocean direction is the compass heading from which waves are arriving for the unidirectional RD, and the mean direction for the spectral RD simulations.

$$\delta(\mathbf{x},\bar{f},\bar{\theta}_0) = E/E_0 \tag{1}$$

the ratio of sheltered wave energy, $E = \int\int df d\theta\, S(f,\theta)$, to deep ocean energy, $E_0 = \int\int df d\theta_0\, S_0(f,\theta_0)$, as a function of the sheltered location, $\mathbf{x}$, the mean deep ocean wave direction, $\bar{\theta}_0$ and mean frequency, $\bar{f}$ of $S_0(f,\theta_0)$. When $S_0(f,\theta_0)$ is a monochromatic, unidirectional plane wave, estimates of δ are often highly variable over directional scales of a few degrees, as illustrated in Fig. 2. Part of this variability is "real" in the sense that a single RD solution represents a single plane wave which, owing to refraction and diffraction around islands and shoals, evolves into waves from multiple directions at a sheltered location. The phase relationships between these multiple wave trains are not random, but defined by the bathymetry. Spatially complex interference patterns occur if the majority of the sheltered wave energy is not from a single direction. Plane waves passing over a circular shoal create a classic and extreme example of such interference patterns. In the far-field of complex bathymetry, these patterns can persist but would be virtually unpredictable in practice. The fixed phase relationships between the wave directions, now many wavelengths away from the bathymetry which modified the wave field,

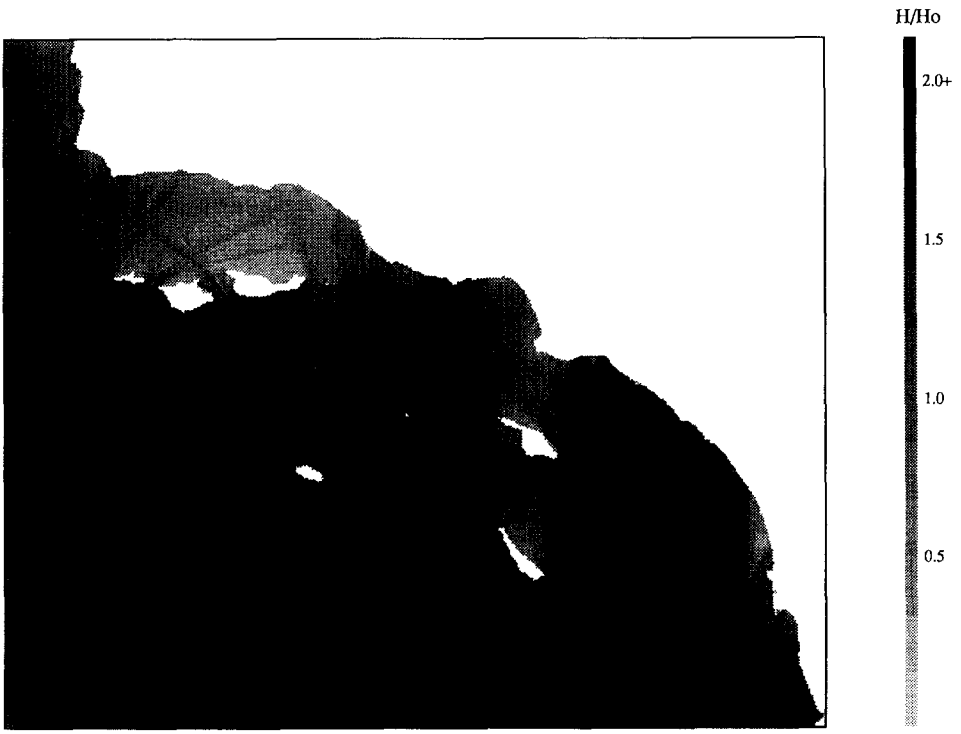

Fig. 3. Relative wave heights predicted by the RD model for a 0.01 Hz (0.055–0.065 Hz), 5° (177.5°–182.5°) rectangular incident wave spectrum. Image has 800 m resolution.

are extremely sensitive to changes in the incident wave frequency and direction, bathymetry grid errors, and the presence of even mild currents or bottom dissipation. Another portion of this variability in δ[O(10%) of S_0] is due to numerical noise. These errors are introduced when energy is dissipated around the islands and when the bathymetry results in wave energy propagating at high angles to the x-axis of the grid (Kirby, 1986a).

If the deep ocean spectrum $S_0(f,\theta_0)$ is approximated as constant over some bandwidth, then estimates of δ obtained by averaging RD model solutions across this band are much smoother (Fig. 2). In the following we discretize the incident deep ocean frequency-directional spectrum into bins of constant energy density, each representing a 0.01 Hz frequency and 5° directional bandwidth, and consider the resulting smoothed δ (Fig. 2). This bandwidth is loosely based on the expected smoothness of the directional spectra of naturally occurring waves. The number of RD model runs required to adequately represent the transformation of a deep ocean spectral bin depends on the complexity of the bathymetry. Up to 90 model runs were averaged to simulate a single bin, and a 25 run average (5 frequencies, 5 directions; $\Delta f = 0.002$ Hz, $\Delta\theta_0 = 1°$) was chosen for the routine computations. The 25 run estimates of δ generally differed from the 90 run average by $< 10\%$. Even with this smoothing, the wave field in the Bight is spatially complex over scales of a few kilometers as illustrated in Fig. 3, depicting the Bight-wide RD model response to a schematic Southern Hemisphere swell.

4. THE SPECTRAL REFRACTION MODEL

Spectral transformations in the Southern California Bight were also performed with the R model derived by Longuet-Higgins (1957) and discussed further by LeMehaute and Wang (1982) and O'Reilly and Guza (1991). If diffractive effects are neglected, the relationship between a spatially homogeneous incident wave spectrum, $S_0(f,\theta_0)$, and a wave spectrum at a shallow water or sheltered location, $S(f,\theta)$, is given by

$$S(f,\theta) = \frac{k}{k_o}\frac{C_{go}}{C_g} S_0(f,\Gamma(f,\theta)) \tag{2}$$

The subscript o refers to the incident wave spectrum, k is the scalar wave number and C_g the group velocity for a given wave frequency and water depth. Equation (2) is valid along a ray path, and the relationship between θ and θ_0 is obtained by back-refracting a directional range of rays from a specific location. LeMehaute and Wang (1982) refer to this relationship as the inverse direction function, Γ, where $\theta_0 = \Gamma(f,\theta)$. The ray back-refraction was performed using a 4th order Runge–Kutta method to integrate the ray equations

$$\frac{dx}{dt} = c\cos\alpha; \quad \frac{dy}{dt} = c\sin\theta; \quad \frac{d\alpha}{dt} = \frac{dc}{dx}\sin\alpha - \frac{dc}{dy}\cos\alpha$$

where α is the direction of wave propagation, and t is time. Wave phase speeds, c, and phase speed gradients are estimated by locally fitting a second degree polynomial surface to a bathymetry grid (Dobson, 1967) with a spacing of 144 m in longitude and 184 m in latitude (i.e. ≈ 1 wavelength in 10 m of water for 0.06 Hz waves). Sub-wavelength variability in the bathymetry is therefore suppressed.

When back-refracted rays strike islands, the associated inverse direction function for sheltered locations, Γ (Eq. 2), is discontinuous, with gaps indicating directions from which deep ocean waves are blocked. Inverse direction functions become very complex when back-refracted rays propagate over large areas with complicated bathymetry. The criteria for selecting the starting directions for back-refracted rays is based on the assumption that the deep ocean directional spectra are approximately constant on scales of 5° in direction at a specific wave frequency. For a given sheltered location, X, rays are initially back-refracted with a local angle increment of 1°. An additional bisecting ray is then computed between two adjacent back-refracted rays that have corresponding deep ocean directions differing by more than 1°. These iterations continue until either all adjacent deep ocean directions are within 1°, or the initial angle increment between two adjacent rays is less than $0.01°/J$, where $J = kC_{go}/k_oC_g$ (Eq. 2) at X. The initial and deep ocean angle criteria are conservatively based on test runs performed at a number of locations throughout the Bight. Similar to the RD model, individual R model runs are combined to define δ (Eq. 1) for rectangular deep ocean spectra with 0.01 Hz–5° bandwidths.

5. SENSITIVITY OF δ TO VARYING TIDAL HEIGHTS

The many possible sources of model errors include the limited linear model physics and errors in the bathymetry grid. Grid inaccuracies are of the greatest concern in shallow water, where the sensitivity of the wave transformations to depth errors is highest and sediment movement is most likely to occur. It is not possible to quantitatively test the models directly because concurrent coastal and detailed deep ocean directional wave data are not available. However, one error that can be crudely simulated is the neglect of tidal changes in water depth. This sensitivity analysis also mimics systematic bathymetry grid errors resulting from survey navigation errors or the movement of large volumes of shallow water sediments. Estimates of δ for several different locations (sheltered deep water and shallow water) and tidal elevations [mean sea level (msl) and ± 1 m from msl], using narrow 0.01 Hz–5° rectangular input (e.g. unsheltered, deep ocean) spectra are shown for R and

RD models in Fig. 4. The variable amounts of wave shoaling ($\approx 5\%$ change in energy) at the shallow water sites with different tidal elevations have been removed. The remaining differences between the transfer functions are due to changes in the wave refraction and refraction-diffraction patterns.

For the R model, tidal fluctuations have little effect on the deep water estimates of δ, but are more important at shallow water sites (e.g. compare left panels in Fig. 4). Typically, the shallow water transfer functions are less stable for the incident directions where local refractive effects result in strong wave energy convergence and large δ. In these cases, small changes in the mean water depth can lead to relatively large changes (20–30%) in δ. This sensitivity to tidal height in shallow water is most pronounced for incident spectra that are narrow in both frequency and direction, as in Fig. 4.

The RD model estimates differ in that they show 20–30% variability with tidal changes at both shallow and deep water locations. Oceanside Deep Water (lower right, Fig. 4) demonstrates that even when a location is far downwave from the effects of islands and shoals, the RD estimate of δ can still be sensi-

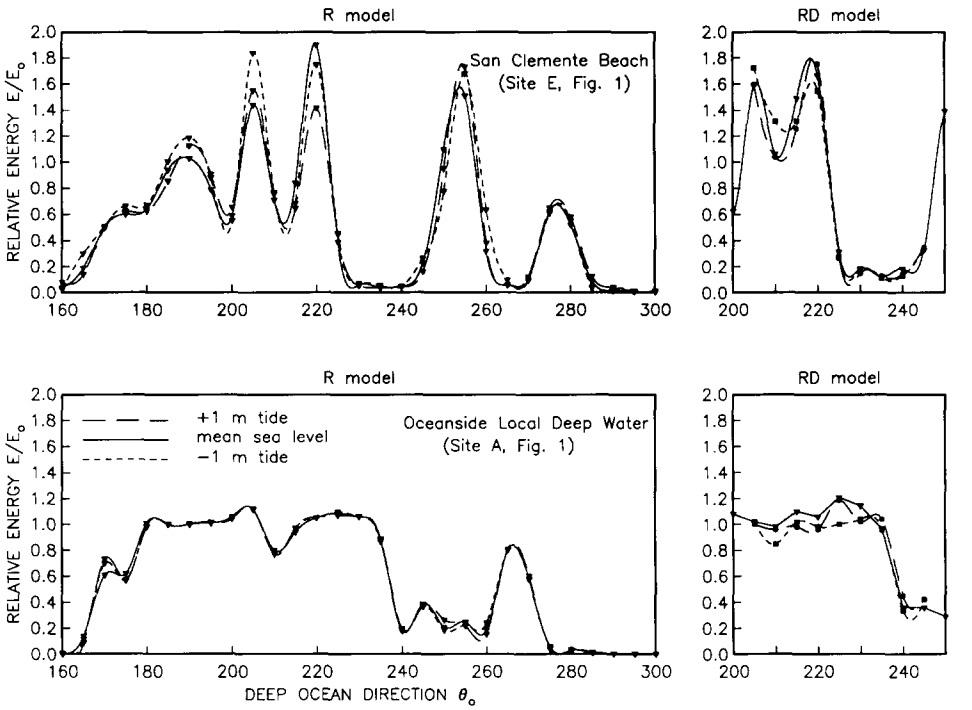

Fig. 4. Sensitivity of R and RD estimates of δ (left and right panels, respectively) at San Clemente Beach and Oceanside Deep Water (top and bottom panels, respectively) to tidal variations. 0.01 Hz–5° rectangular deep ocean spectrum, $f = 0.055$–0.065 Hz. RD model simulations are only shown for the southwest grid orientation; $205° < \theta_0 < 245°$.

tive to relatively small water depth changes over the entire grid, even with smoothing over a 0.01 Hz–5° bandwidth. Most of this sensitivity occurs because RD interference patterns many wavelengths away from the refraction-diffraction sources are shifted spatially by relatively small depth changes. The R model suppresses these interference patterns in sheltered deep water (compare lower panels in Fig. 4 and see O'Reilly and Guza, 1991), thus R solutions are more stable than RD solutions, although not necessarily more accurate. Additional results show that as the wave spectrum becomes broader in frequency or direction, interference patterns are blurred by averaging, and the resulting smooth patterns are much less sensitive to tidal fluctuations.

Modifying the models to include tides is computationally prohibitive because the wave travel time from the offshore banks and islands to the coast is a significant portion of a tidal cycle. Therefore tidal effects cannot be accurately represented by simply changing the sea level elevation of the entire Bight for a specific model run (as in Fig. 4). Instead, depths in the model would need to be progressively correct as the model solution propagated across the grid, and many additional model runs for each frequency and wave direction would be needed to cover the range of possible tide scenarios.

6. SENSITIVITY OF δ TO DIFFERENCES IN THE WAVE MODELS

One drawback of the present RD model is that it is difficult, if not impossible, to accurately estimate directional spectra within the Bight because the directional calculations are very sensitive to numerical noise in the RD results (O'Reilly and Guza, 1991). Therefore, in its present form, the RD model is limited to estimating frequency spectra. The R model predicts frequency-directional spectra within the Bight in a more straightforward manner (Eq. 2). Additionally, if estimates of δ are needed at only a few sites within a large numerical domain, then the R model solutions can be computed much faster than the RD solutions.

Therefore, we compared R and RD energy transfer functions at representative locations, including 3 sheltered deep water sites (sites A, B, and C in Fig. 1) that are close to the mainland and in the far-field of the islands and offshore banks. Energy transfer functions at these sites are shown in Figs. 5–7 for rectangular deep ocean wave spectra which are 0.01 Hz wide in frequency (0.055–0.065 Hz) and have narrow and broad directional widths (5° and 25°). Sites A and B are partially sheltered by offshore banks and islands and δ varies significantly with θ_0 for narrow incident spectra (Figs. 5 and 6, upper panels). One example of the differences between the models is Oceanside Deep Water (site A) for the incident direction of 210° (Fig. 5, upper panel), an angle for which waves pass over the 60 and 40 Mile Banks (Fig. 1) before reaching the coast. The reduction of the R model estimate of δ relative to RD is analogous to the circular shoal example in O'Reilly and Guza (1991),

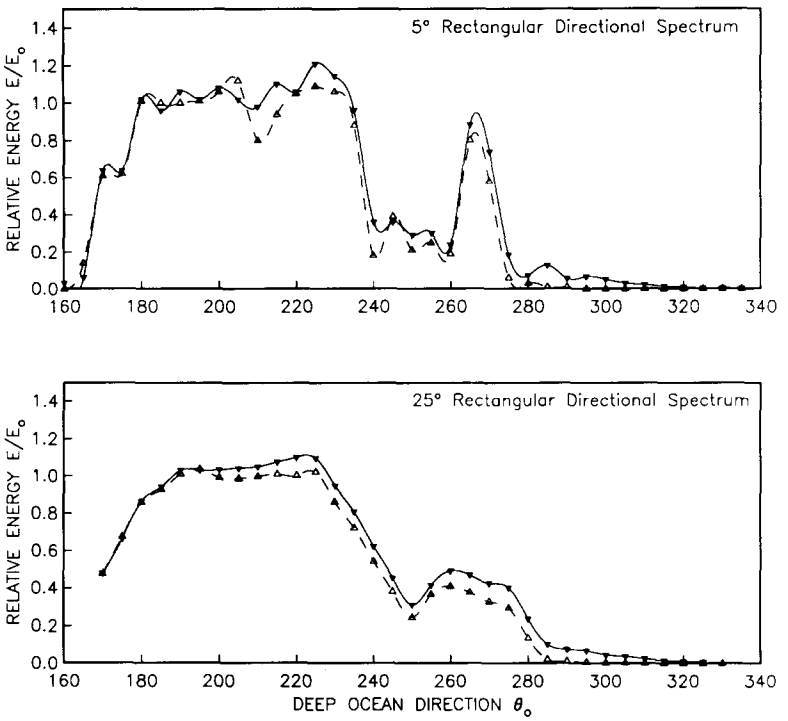

Fig. 5. Oceanside Local Deep Water (Site A, Fig. 1). Solid = RD, dashed = R model. $f = 0.055$–0.065 Hz.

where the R model also underestimates the wave energy directly downwave of the shoal.

The Santa Monica Bay region (the area near Site B, Fig. 1) has a particularly complex wave climate due to its exposure to offshore shoals such as Cortez and Tanner Banks, and the shallow bathymetry around San Nicolas and Santa Barbara Islands. This results in a very complicated δ at Santa Monica Deep Water and greater differences between the two models than at Oceanside (compare Figs. 5 and 6, upper panels). For a narrow incident spectrum, the R model both over and underestimates δ, compared to RD, while capturing the same major features (Figs. 6). As the deep ocean spectrum becomes broader, the solutions converge to similar smooth estimates of δ at both sites (Fig. 5 and 6). In the cases of broad directional spread, the R model estimate of δ is usually lower than RD. This bias is most likely due to numerical noise in the RD solutions, produced when wave energy is dissipated around islands or when the bathymetry results in waves propagating at high-angles to the x-axis of the grid (Kirby, 1986a). The solutions were not filtered, so the spurious noise is superimposed on the actual wave field, and this introduces a positive bias when averaged into the RD spectral estimates. It is interesting

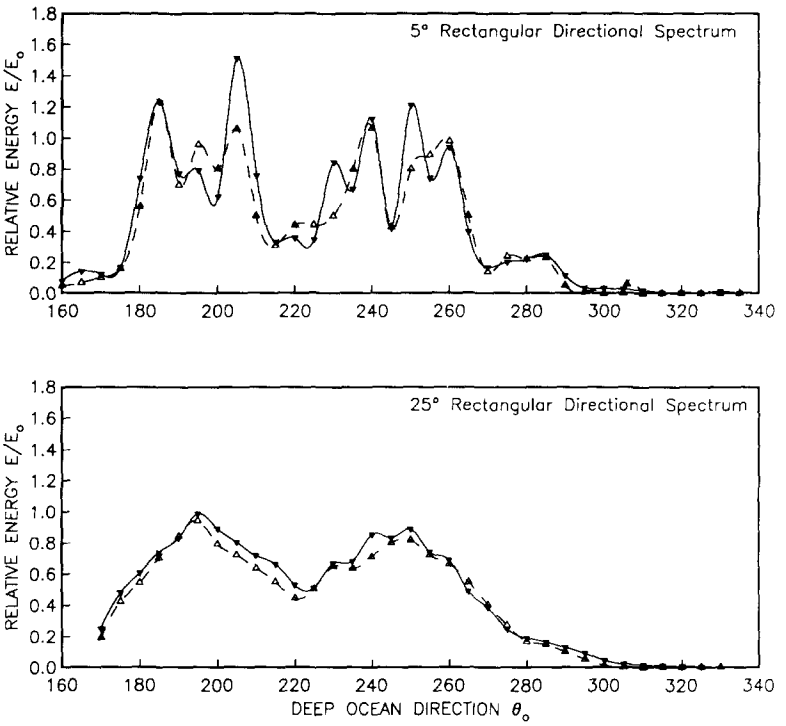

Fig. 6. Santa Monica Local Deep Water (Site B, Fig. 1). Solid = RD, dashed = R model. f = 0.055–0.065 Hz.

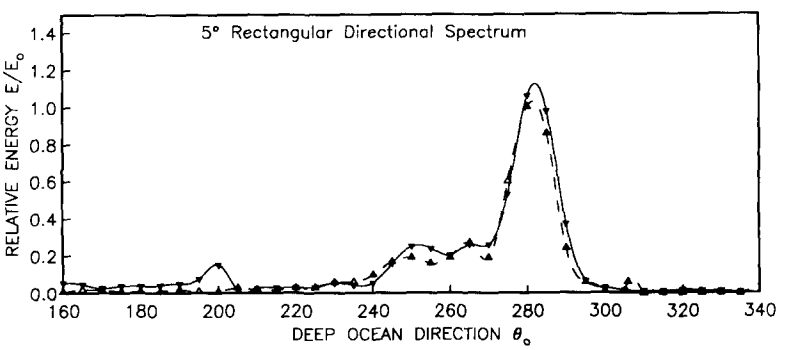

Fig. 7. Santa Barbara Local Deep Water (Site C, Fig. 1). Solid = RD, dashed = R model. f = 0.055–0.065 Hz.

that Izumiya and Horikawa (1987) also showed slightly larger RD estimates when comparing R and RD models over parallel bathymetry contours; however, the RD model should be essentially "noise free" in their case.

Both models predict the same main feature at Santa Barbara (Site C, Fig. 1), even in the narrow spectrum case (Fig. 7). Unlike the two previous loca-

tions, site C is not exposed to complicated bathymetry because of total blocking by Santa Cruz Island directly to the south. Significant amounts of wave energy can only reach the site from the west, with few shoals or complex bathymetric features to induce wave diffraction.

For a given section of coastline, model differences at shallow water sites tend to be slightly larger than the differences in deeper water (e.g. compare Oceanside deep, Fig. 5, to Oceanside and San Clemente shallow, Figs. 8 and 9). This is consistent with the increased importance of local diffractive effects in shallow water. As was the case for the deep water sites, the model agreement improves substantially with broader incident directional spectra (Figs. 8 and 9, lower panels). However, unlike the deeper locations, there is no clear bias in the RD model estimates of energy.

We expected the very rough bathymetry of the Redondo Submarine Canyon (Site F, Fig. 1) to render the R model nearly useless. Although the differences in the estimated maxima of δ are substantial, the R model did a surprisingly good job of identifying the most highly amplified deep ocean wave directions for sites around the head of the canyon (e.g. Fig. 10). Thus the smoothing associated with even a narrow 0.01 Hz–5° bandwidth brought the R and RD models into better than anticipated agreement.

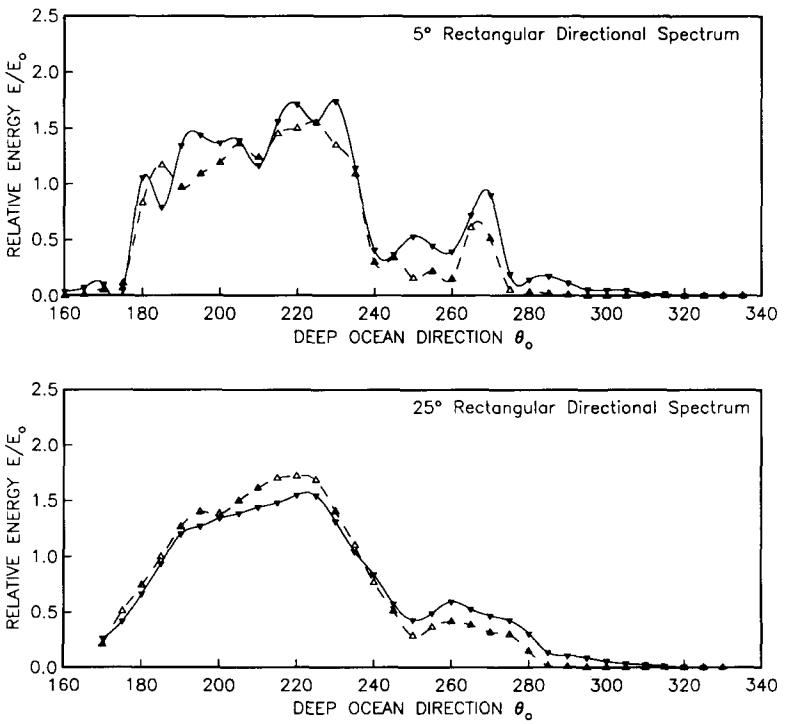

Fig. 8. Oceanside Beach (Site D, Fig. 1). Solid = RD, dashed = R model. f = 0.055–0.065 Hz.

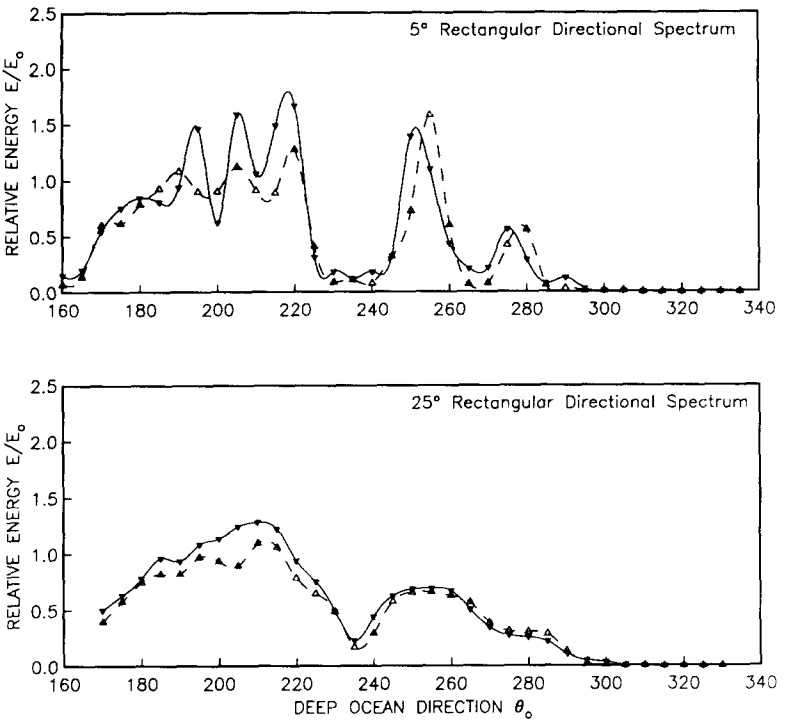

Fig. 9. San Clemente Beach (Site E, Fig. 1). Solid = RD, dashed = R model. $f = 0.055$–0.065 Hz.

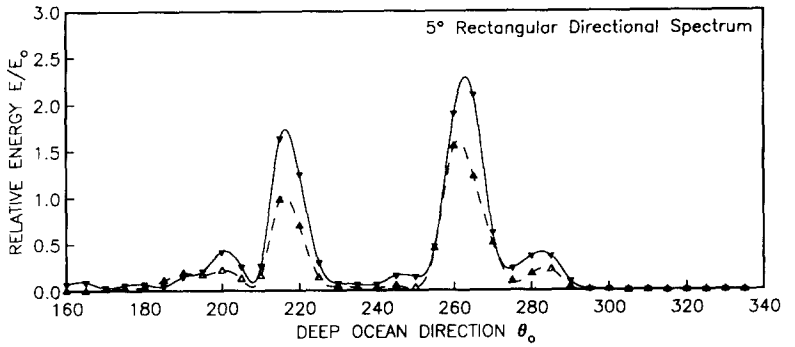

Fig. 10. Redondo Submarine Canyon, near north end of King Harbor breakwater (Site F, Fig. 1). Solid = RD, dashed = R model. $f = 0.055$–0.065 Hz.

7. SENSITIVITY OF δ TO ERRORS IN THE INCIDENT DIRECTIONAL SPECTRUM

As is often the case when using numerical models to describe physical processes, it is much easier to apply the model to a particular problem than to verify the accuracy of the results. Due to the directional sensitivity of the

island sheltering processes, model verification through comparisons to field measurements is not straightforward even though there is a relatively large amount of wave energy and slope array data for locations within the Bight. Figures 4–10 show that sheltered wave energy estimates are sensitive to relatively small changes in wave direction and thus to small errors in specifying $S_0(f,\theta_0)$. Unfortunately, high resolution deep ocean directional wave spectra are not available. Coastal engineers often use wave hindcasts as a source of historical deep water wave information. However, most hindcasts provide only rough directional information (e.g. approximate peak directions and directional spread information), and the accuracy of higher resolution spectral hindcast models is unknown.

The main source of in-situ directional wave information, the pitch-and-roll buoy, provides a fundamentally low-resolution estimate of wave directionality. Figure 11 shows two directional distributions, one bimodal and the other more unimodal, which both fit the same error free pitch-and-roll data exactly [Ochoa and Gonzalez (1990) discuss a variety of directional spectra which are consistent with the same pitch-and-roll data]. The 0.01 Hz–5° rectangular incident spectra of the previous examples were replaced by these distributions, and R and RD estimates of δ for two sheltered sites are shown in Fig. 12. The differences in δ due to different interpretations of the buoy data (i.e.

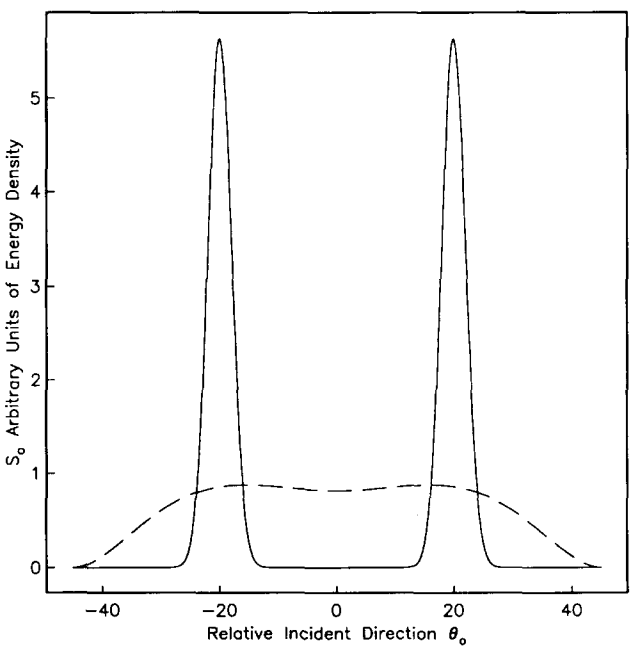

Fig. 11. Bimodal (solid) and unimodal (dashed) directional spectra, f=0.055–0.065 Hz. Both spectra exactly fit the same error-free pitch-and-roll data.

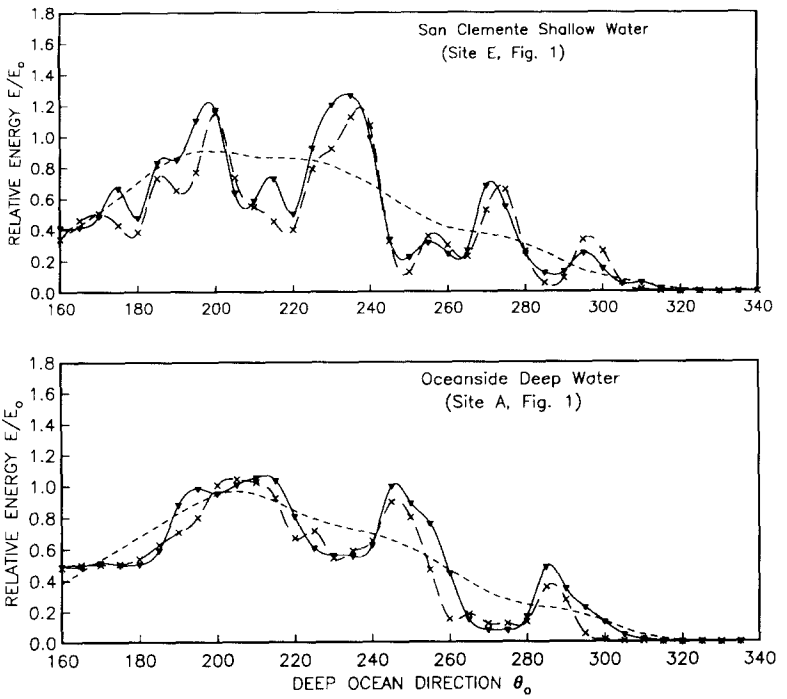

Fig. 12. R and RD estimates of δ based on the bimodal and unimodal spectra of Fig. 11. RD bimodal (solid); R bimodal (long dashes); RD unimodal (short dashes).

unimodal or bimodal) are larger than differences between the R and RD models for the bimodal shape. Pitch-and-roll buoy measurements can be quite useful, however, because of their directional uncertainty, they cannot not be confidently used as input to wave transformation models without additional information. For example, if it is known that the deep ocean spectrum was generated by a single, nearby storm, then a broad, unimodal estimate of $S_0(f,\theta_0)$ from a directional buoy may be adequate. The wave propagation models are least sensitive to errors in broad spectra, so the best estimates of sheltered wave energy would be made under these circumstances. However, we believe that the overall quality of available deep ocean wave data will often be the limiting factor in studies of wave propagation over complex bathymetry like that found in Southern California.

8. TWO-DIMENSIONAL ENERGY TRANSFER FUNCTIONS

The two-dimensional energy transfer function for site D (Fig. 1), calculated using the R model, is contoured in Fig. 13, covering wave frequencies from 0.05 Hz to 0.12 Hz (periods from approximately 8 to 20 seconds), as well as the range of important incident deep ocean wave directions. The

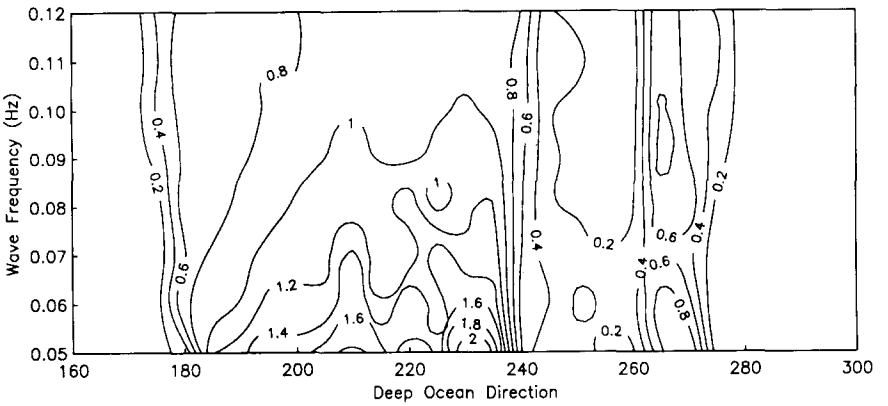

Fig. 13. Two-dimensional energy transfer function for Oceanside Beach (Site D, Fig. 1). Contours are of relative energy (E/E_0) for a 5°–0.01 Hz incident wave spectrum centered on a given frequency and direction.

transfer function shown is for the narrow deep ocean spectra used previously (i.e. the 0.055–0.065 Hz band is shown in the upper panel of Fig. 8).

For coastal engineering applications, 2-D wave energy transfer functions (e.g. Fig. 13) take full advantage of the linear wave model results, and provide additional information about extreme wave events when applied in conjunction with wave hindcasting theory. More specifically, transfer functions and estimates of possible directional and frequency distributions of deep ocean wave energy can be combined to estimate the largest plausible amplifications of the offshore wave energy at shallow water sites. These estimates can differ significantly from the largest coastal wave energies that have occurred in recent history. This is particularly evident along partially sheltered coastlines, where the direction and width of the offshore spectrum can be as important as the total energy.

For example, Seymour et al. (1984) compiled a hindcast of wave events (1900–1984) with significant heights > 6 m at unsheltered location seawards of the islands. The largest event ($H_s = 8.8$ m) had a hindcast peak frequency and direction of 0.065 Hz and 247° respectively. Assuming for the point of illustration that the deep ocean spectrum was narrow, Oceanside Beach was significantly sheltered from this event (Fig. 13, $\delta = E/E_0 \approx 0.3$). However, a plausible 12° shift in the peak incident direction to 235° would result in $\delta \approx 1.4$.

Not surprisingly, larger amplifications of the deep ocean wave energy occur at the lower wave frequencies where wave transformations and shoaling are enhanced for a given shallow bathymetry. The largest amplification (≈ 2.0) results when the narrow incident spectrum is centered on a wave frequency of 0.05 Hz and a direction of ≈230–235° (Fig. 13). Assuming directional widths are not less than 5°, this is an upper bound on the amplification of

deep ocean swell (a wider spectrum spreads the deep ocean wave energy over neighboring deep ocean directions and frequencies and reduces the amplification effect through averaging).

9. DISCUSSION

Simulations show that RD model estimates of energy transfer functions, δ, contain a positive bias [$O(10\%)S_0$] at many sheltered locations due to numerical noise (Figs. 5–9, lower panels). In addition, RD errors can result from simulating the transformation of a deep ocean spectrum as an average of unidirectional RD model runs [these errors are $<10\%$) for the 1°–0.002 Hz model resolution used here]. Both models are moderately sensitive to tidal fluctuations and/or possible systematic errors in the bathymetry grid [$O(20$–$30\%)S_0$], although the R model is only sensitive in shallow water (Fig. 4).

Comparisons of the two models at various locations throughout the Bight show differences that are of the same order as the tidal fluctuation errors for narrow incident wave spectra (compare Fig. 4 to Figs. 5–9, upper panels). As might be expected, model agreement in a particular region is better in deeper waters, away from shallow water diffractive effects. If the true incident waves were a unidirectional, monochromatic plane wave, then the resulting wave field would be essentially unpredictable in a large complex region such as the Bight (Fig. 2). As the incident spectrum becomes broader in frequency and direction, the model solutions become smoother and more similar (Figs. 5–9, lower panels). In O'Reilly and Guza (1991), the R model showed poorer agreement with RD, compared to the present examples, for narrow spectra with simple natural bathymetry. However, a finite frequency bandwidth was not used in the previous simulations and this additional smoothing improves the model agreement. The sensitivity of δ to small changes in direction, and simulations with two different incident wave directional spectra (both consistent with the same pitch-and-roll buoy data), showed that model errors due to uncertainty in the input directional spectrum can be larger than the differences between the models themselves (Fig. 12).

The model comparisons are useful in evaluating model deficiencies. For example, the R model cannot simulate wave diffraction. Many investigators have studied the diffraction of wave energy around islands, and Pawka (1983) specifically addressed this problem within the Bight. His conclusion, that the effects of island edge diffraction are small in the far-field of the islands, is supported by the comparisons of the models in sheltered deep water (Figs. 5–7). Some of the largest deep water differences between the models are not due to island edge diffraction, but instead are a result of diffraction over some of the offshore shoals such as 40 and 60 Mile Bank (Fig. 1). The R model underestimates wave energy directly downwave of these features. The comparisons also demonstrate that high-angle wave propagation errors in the RD model

can be reduced to a O(10%)S_0 positive bias using several different grid orientations. One of the most common criticisms of the parabolic equation method is the potential impact of these high-angle errors, yet this bias is relatively small when the RD model is used to simulate spectra rather than unidirectional waves. However, the resulting numerical noise in the RD model limit it to predictions of frequency spectra rather than full directional spectra, and for highly sheltered locations, neither model is likely to provide quantitative estimates of the low energy conditions. We found the R model to be surprisingly robust owing to finite distributions of wave energy in both frequency and direction. Even with features as complicated as submarine canyons, the R model correctly identified the most highly amplified deep ocean wave directions (Fig. 10).

The sensitivity of the transformation process to details of $S_0(f,\theta_0)$, along with the known uncertainty in the available estimates, precludes direct verification of the models. O'Reilly (1991) has used inverse methods to show that deep ocean directional distributions can be found that are consistent with hindcasts, the numerical models, and (limited) sheltered wave measurements. More definitive field tests of the models are underway.

ACKNOWLEDGEMENTS

This research was supported jointly by the California Department of Boating and Waterways, as part of its ongoing wave data applications program, and Sea Grant. Our thanks to Eloi Melo, Universidade Federal do Rio de Janeiro, Brazil, for his assistance in developing the RD model used in this study. Support for the RD model calculations was provided by the San Diego Supercomputer Center.

This work is the result of research sponsored in part by the National Oceanic and Atmospheric Administration, National Sea Grant College Program, Department of Commerce, under grant number NA89AA-D-SG138, project number R/CZ-90, through the California Sea Grant College, and in part the California State Resources Agency. The U.S. Government is authorized to reproduce and distribute this report for governmental purposes.

REFERENCES

Arthur, R.S., 1951. The effect of islands on surface waves. SIO Bull., 6(1): 1–26.

Dalrymple, R.A., Kirby, J.T. and Hwang, P.A., 1984. Wave diffraction due to areas of energy dissipation. J. Waterway, Port, Coastal Ocean Eng., 110(1): 67–79.

Dobson, R.S., 1967. Some applications of the digital computer to hydraulic engineering problems. Tech. Rep. 80, Dept. Civil Eng., Stanford Univ.

Emery, K.O., 1958. Wave patterns off Southern California. J. Marine Res., 17: 133–140.

Isobe, M., 1987. A parabolic model for transformation of irregular waves due to refraction, diffraction and breaking. Coastal Eng. Jpn., 30(1): 33–47.

Izumiya, T. and Horikawa, K., 1987. On the transformation of directional random waves under combined refraction and diffraction. Coastal Eng. Jpn., 30(1): 49–65.

Kirby, J.T., 1986a. Higher-order approximations in the parabolic equation method for water waves. J. Geophys. Res., 91 (C1): 933–952.

Kirby, J.T., 1986b. Open boundary condition in the parabolic equation method. J. Waterway, Port, Coastal Ocean Eng., 112(3): 460–465.

Kirby, J.T. and Dalrymple, R.A., 1986. Modeling waves in surfzones and around islands. J. Waterway, Port, Coastal Ocean Eng., 112(1): 78–93.

LeMehaute, B. and Wang, J.D., 1982. Wave spectrum changes on a sloped beach. J. Waterway, Port, Coastal Ocean Eng., 108(WW1): 33–47.

Longuet-Higgins, M.S., 1957. On the transformation of a continuous spectrum by refraction. Proc. Cambridge Philos. Soc., 53(1): 226–229.

Munk, W.H. and Traylor, M.A., 1947. Refraction of ocean waves: A process linking underwater topography to beach erosion. J. Geol., 55(1): 1–26.

Ochoa, J. and Gonzalez, O.E.D., 1990. Pitfalls in the estimation of wind wave directional spectra by variational principles. Appl. Ocean Res., 12(4): 180–187.

O'Reilly, W.C. and Guza, R.T., 1991. Comparison of spectral refraction and refraction–diffraction wave models. J. Waterway, Port, Coastal Ocean Eng., 117(3): 199–215.

O'Reilly, W.C., 1991. Modeling surface gravity waves in the Southern California Bight. Ph.D. Dissertation, Univ. of California, San Diego, 90 pp.

Panchang, V.G., Weil, G., Pierce, B.R. and Briggs, M.J., 1990. Numerical simulation of irregular wave propagation over a shoal. J. Waterway, Port, Coastal Ocean Eng., 116(3): 324–340.

Pawka, S.S., 1982. Wave directional characteristics on a partially sheltered coast. Ph.D. Dissertation, Univ. of California, San Diego, 246 pp.

Pawka, S.S., 1983. Island shadows in wave directional spectra. J. Geophys. Res., 88(C4): 2579–2591.

Seymour, R.J., Strange, R.R., Cayan, D.R. and Nathan, R.A., 1984. Influence of El Ninos on California's wave climate. Proc. 19th Int. Conf. Coastal Eng., Houston, TX, ASCE, Vol. 1, pp. 577–592.

Watson, D.F., 1982. ACORD: Automatic contouring of raw data. Comput. Geosci., 8(1): 97–101.